



HAL
open science

Measured density of copper atoms in the ground and metastable states in argon magnetron discharge correlated with the deposition rate

H Naghshara, S Sobhanian, S Khorram, N Sadeghi

► **To cite this version:**

H Naghshara, S Sobhanian, S Khorram, N Sadeghi. Measured density of copper atoms in the ground and metastable states in argon magnetron discharge correlated with the deposition rate. *Journal of Physics D: Applied Physics*, 2011, 44 (2), pp.25202. 10.1088/0022-3727/44/2/025202 . hal-00597851

HAL Id: hal-00597851

<https://hal.science/hal-00597851>

Submitted on 2 Jun 2011

HAL is a multi-disciplinary open access archive for the deposit and dissemination of scientific research documents, whether they are published or not. The documents may come from teaching and research institutions in France or abroad, or from public or private research centers.

L'archive ouverte pluridisciplinaire **HAL**, est destinée au dépôt et à la diffusion de documents scientifiques de niveau recherche, publiés ou non, émanant des établissements d'enseignement et de recherche français ou étrangers, des laboratoires publics ou privés.

Measured density of copper atoms in the ground and metastable states in argon magnetron discharge correlated to the deposition rate

H. Naghshara¹, S. Sobhanian¹, S. Khorram¹ and N. Sadeghi^{2,a}

- 1) Faculty of Physics, University of Tabriz, Tabriz, Iran
- 2) LSP, Université Joseph Fourier & CNRS, Grenoble, France

PACS : 52.2.Hv ; 52.70. Kz ; 52.80.Sm ; 32.70.Jz

Abstract:

In a dc-magnetron discharge with argon feed gas, densities of copper atoms in the ground state $\text{Cu}(^2\text{S}_{1/2})$ and metastable state $\text{Cu}^*(^2\text{D}_{5/2})$ were measured by resonance absorption technique, using a commercial hollow cathode lamp as light source. The operating conditions were 0.3 - 14 μbar argon pressure and 10 - 200 W magnetron discharge power. The deposition rate of copper in a substrate positioned at 18 cm from the target was also measured with a quartz microbalance. The gas temperature, in the range of 300 to 380 K, was deduced from the emission spectral profile of $\text{N}_2(\text{C}^3\Pi_u - \text{B}^3\Pi_g)$ 0-0 band at 337 nm when trace of nitrogen was added to the argon feed gas. The isotope-shifts and hyperfine structures of electronic states of Cu have been taken into account to deduce the emission and absorption line profiles, and hence for the determination of atoms densities from the measured absorption rates. To prevent error in evaluation of Cu density, attributed to the line profile distortion by autoabsorption inside the lamp, the lamp current was limited to 5 mA. Density of $\text{Cu}(^2\text{S}_{1/2})$ atoms and deposition rate both increased with the enhanced magnetron discharge power but at fixed power the copper density augmented with argon pressure whereas the deposition rate followed the opposite trend. Whatever the gas pressure, the density of $\text{Cu}^*(^2\text{D}_{5/2})$ metastable atoms remained below the detection limit of $1 \times 10^{10} \text{ cm}^{-3}$ for magnetron discharge powers below 50 W and hence increased much rapidly than the density of $\text{Cu}(^2\text{S}_{1/2})$ atoms, over passing this later at some discharge power, whose value decreases with increasing argon pressure. This behavior is believed to result from the enhancement of plasma density with increasing discharge power and argon pressure, which would increase the excitation rate of copper into metastable states. At fixed pressure, the deposition rate followed the same trend than the total density of copper atoms in the ground and metastable states. Two important conclusions of this work are: *i*) copper atoms sputtered from the target under ion bombardment are almost all in the ground state $\text{Cu}(^2\text{S}_{1/2})$ and hence in the plasma volume they can be excited into the metastable states; *ii*) all atoms in the long-lived ground and metastable states contributes to the deposition of copper layer on the substrate.

^a Corresponding author ; E-mail : nader.sadeghi@ujf-grenoble.fr

1- Introduction

Magnetron discharges are widely used for thin film deposition in surface treatment^{1, 2}, magnetic and superconducting devices³, semiconductor industry⁴ and in surface coating engineering of materials under low temperature conditions^{5, 6}. In these systems, the magnetic field, usually produced by placing permanent magnets behind the cathode, confines the plasma in the near cathode region, reducing the electron loss to the sidewalls. By increasing the ionization rate near the cathode, which is also the target to be sputtered, its confinement helps to maintain the plasma at much lower buffer gas pressure than in a normal dc discharges. Bombardment of the target by ions leads to the sputtering of metal atoms, which then diffuse in the plasma volume and are partly deposited in the substrate positioned at about tens of cm from the target. So, in spite of small current densities, high metal atom production rates are achieved by magnetron discharges. Also, the high stability and uniformity of these plasmas are another factor for the success of these systems. But uniform, high quality and damage-free layer deposition requires the deep understanding of the gas phase processes in magnetron plasma, sputtering processes from the target, and deposition processes on the substrate. In particular, it is of prime importance to identify different electronic states of the metal, copper in the present case, which are highly populated. Beside the ground state, metastable states of copper, from which optical transition to the ground state is forbidden, must therefore be considered. The most popular diagnostic tools to characterize the plasma volume and control the discharge parameter are optical emission and absorption techniques. Britum *et al* have used a Fabry-Perot interferometer to deduce the gas temperature in argon magnetron discharges with different target materials⁷, or to record the velocity distribution function of sputtered metal atoms⁸. The same group characterized a titanium magnetron discharge by using the resonance absorption technique, with a hollow cathode lamp⁹ or the laser induced fluorescence technique¹⁰. Using the space and time resolved laser induced fluorescence technique in magnetron plasmas of different target materials (Fe, Ti, Cu) and rare gases (Ar, Kr, Xe), Sasaki *et al* have suggested that dimmers and trimers of metal atoms could also be sputtered from the target and get dissociated in the plasma volume¹¹. The space resolved electron density and energy distribution function of electrons have also been obtained with a Langmuir probe in several magnetron systems^{12, 13, 14}.

In this work the emission spectroscopy of nitrogen, added as trace to the argon buffer gas, is used for monitoring the gas temperature and the resonance absorption spectroscopy, with a commercial hollow cathode lamp as light source, is employed for the measurement of copper atoms densities in the ground state $\text{Cu}(^2\text{S}_{1/2})$ and metastable state $\text{Cu}^*(^2\text{D}_{5/2})$. Figure (1) shows the simplified energy levels of copper involved in this work. Due to the presence of two isotopes in copper and a $I=3/2$ nuclear spin in both isotopes, the electronic states of copper are split in different sub-levels. Consequently, the precise determination of atoms densities from absorption measurements requires an exact treatment of the absorption phenomenon for a multi-line transition.

This paper is organized as following: Experimental set-up and measurement techniques are presented in section 2. Section 3 deals with gas temperature measurements. Principles of resonance absorption spectroscopy and its application to multicomponent lines are developed in section 4 and in Appendix A. The influence of the magnitude of the current

running the hollow cathode lamp, used for the absorption measurements and the effective temperature of the lamp are shown in section 5. Results relative to the variation of copper deposition rate on the substrate and of $\text{Cu}(^2\text{S}_{1/2})$ and $\text{Cu}^*(^2\text{D}_{5/2})$ densities in the plasma volume are reported in sections 6 and 7, respectively and conclusions derived from these results are presented and discussed in section 8.

2- Experimental

The experimental set-up is shown in figure 2. The magnetron used in this study consists of a 60 cm diameter, 50 cm high stainless steel chamber (MECA-2000 Sputtering System) equipped with two 7.5 cm diameter water cooled targets. One of the targets is connected to a Radio Frequency source for the plasma excitation in the RF mode and the other target, which is the only one used in this work, is made of 99% pure copper disk connected to a high voltage dc source. Around each target, the unbalanced magnetic field, produced by 22 permanent magnets, has a conventional structure¹⁵ with 40 mTesla strength at the target surface. The distance from the target to the chamber base is 12 cm and the distance from the target axis to either chamber axis and chamber wall is 15 cm. The pumping system, composed of a 900 l/s turbomolecular pump (ATP900 Alcatel) backed by a 30 m³/hour rotary pump (2033SD Alcatel), can provide a base pressure down to 5×10^{-5} mbar inside the chamber. Argon (99.999% purity) is admitted into the chamber with a flow rate of 25 sccm and a throttle valve, located in the entrance of the turbo pump, maintain the chamber pressure, measured with a capacitance gauge, to a pre-set value in the range of 0.3 to 14 μ bar. The plasma is produced by applying a negative high voltage to the target, the grounded chamber walls acting as anode. The dc magnetron power is automatically set to its pre-fixed value (up to 1 kW) by the adjustment of the applied dc voltage. Up to 220 W power is used in the present work, for which the voltage is ranging between 280 and 400 V. To ascertain the gas purity in the magnetron chamber during optical measurements, argon flows through the magnetron chamber for about 5 minutes before each data acquisition series and the gas purity is checked from the absence of nitrogen bands in the light from the magnetron discharge. For the gas temperature measurements from the rotational structure of N_2 molecular bands, a few per cent of nitrogen is added to the argon feed gas. The 10 cm diameter substrate holder is located at the same radial position than the target at 18 cm above it. The deposition rate to the substrate of the sputtered metal atoms is measured with a quartz microbalance, located at the same level than the substrate and at close distance to it.

Observed visually, the plasma expands in front of the target and, depending on the gas pressure, the plasma diameter increases with the distance from the target. The chamber has several viewports; two of them positioned along a diagonal are equipped with 2.5 cm diameter quartz windows for optical diagnostics. The axis of these windows is positioned at 10 cm above the target, where the plasma is almost homogeneous, within the 20 cm long Cu density measurement volume (see below), for the all studied conditions. Density of copper atoms is measured by resonance absorption technique, with the probe beam from a copper hollow cathode lamp crossing the plasma chamber through the windows (see Fig. 2). To limit the monitoring zone to the homogeneous part of the plasma, two 1.25 cm inner diameter tubes are positioned inside the chamber along the observation

windows axis. The one located in the magnetron discharge side is 5 cm long and the other one is 35 cm long, providing between them 20 cm absorption length through the plasma. These tubes also protect the windows from the metal deposition. For the resonance absorption measurements, a 2.5 cm diameter, 10 cm focal length quartz lens provides a parallel light beam from a commercial copper hollow cathode lamp (HCL). After crossing the plasma chamber through the limiting tubes, the beam is focused with a 2.5 cm diameter, 5 cm focal length quartz lens into the entrance slit of a HR-320 monochromator (Jobin-Yvon), equipped with a 2400 groves/mm grating. Both entrance and exit slits widths are set to 100 μm , providing a spectral resolution of about 0.14 nm, full width at half maximum (FWHM). The light is then detected with a photomultiplier tube (Electron Tubes Limited model P25232-05) working in the photon counting mode. For absorption measurements, the monochromator is set on one of the copper lines (324.7 nm, 327.4 nm or 510.6 nm). To extract the absorption signal from the light received by the PMT, the emission of the hollow cathode lamp is square wave modulated at 10 Hz, by modulating the voltage applied to the lamp with a MOSFET relay in its power supplier (14 in Fig. 2). A 38 k Ω resistor limits the HCL current. In every 50 ms half period of the square wave, 5ms after the HCL current is turned on or off, the main generator (13 in Fig. 2) sends a pulse to the PMT controller which turns on for 35ms its high voltage. The number of photons counted during this period of time is then recorded to the computer and the counter is reset to zero, waiting for the next count signal from the main generator. So, one out of the two following records corresponds to the plasma emission (when the HCL is off) and the other one (when the HCL is on) represents the light from the HCL, transmitted through the plasma, plus the plasma emission. Finally, a file, with the sample numbers in the first column and the corresponding photon counts in the second column, is built and stored in the computer. As an example, Figures 3 and 4 show the recorded data for the 510.6 nm and 327.4 nm lines when the magnetron power was progressively enhanced up to 220 W, by steps of 10 or 20 W. Each record starts with the magnetron plasma turned off, under which conditions the difference between the mean values of the HCL on time data (upper trace) and the HCL off time data (lower trace) provides the unabsorbed intensity I_0 . The dark count rate of the PMT, S_{BG} , is also deduced from the HCL off time data. After $t \approx 20$ seconds of data acquisition ($20 * t$ samples), the magnetron plasma is turned on at 10 W. The corresponding intensity change is clearly seen at sample number around 200 of the 327.4 nm record of Fig. 4. The signal is so recorded during 20-30 seconds for each discharge power before this later is increased again by 10 or 20 W. In the inset of Figure 3, the successively recorded photon counts and their changes at sample 2905, when the plasma power is increased from 70 to 80 W, are easily identified. At each plasma power W , the difference between the mean values of the HCL on period records (upper trace) and the HCL off period records (lower trace) provides the corresponding transmitted intensity $I(W)$. The absorption rate, $A(W)$ at power W is deduced from the relation¹⁶: $A(W) = 1 - (I(W)/I_0)$. Also, the difference between the HCL off period count and S_{BG} is proportional to the plasma emission signal at this power. The last records on each file are with the plasma turned off again and I_0 deduced from these records permits to verify the stability of the HCL emission signal.

3- Gas temperature

As it will be discussed in the following section, the determination of absorbing atoms density requires the knowledge of the Doppler width of the absorption line, hence the kinetic temperature of these atoms. A very reliable method to obtain the gas temperature is from the linewidth of the Doppler-broadened absorption profile of a specific line, measured with a single-mode tunable diode laser. Absorption from argon metastable atoms is particularly popular in pure argon plasmas^{17,18,19,20} or by adding a small amount of argon to the halogen based plasmas²¹. Another commonly used technique consists of adding a small amount of a diatomic molecule, very often N₂, to the plasma and on the measurement of its rotational temperature. This temperature, deduced from the emission intensity of the rotational lines of N₂(C³Π_u- B³Π_g) transition, is assumed to be in equilibrium with the kinetic energy of the bath gas²². The strong 0-0 band of the second positive system at 337.1 nm, originating from the C³Π_u state is often chosen to probe the rotational distribution of this state. However, in argon plasmas, especially at low electron density conditions, the N₂ C; v'=0 level is also populated by the energy transfer reaction from the most abundant Ar*(³P₂) metastable atoms, which preferentially populates the high rotational levels (up to J = 55) of the C; v'=0 level, resulting in an 'effective rotational temperature' of about 2300 K^{23,24}. Extended discussion on Boltzmann equilibrium in rotational levels by collisional transfers evidenced that in argon plasmas the equilibrium is barely reached and the high rotational levels of the C; v'=0 state always remain overpopulated²⁵. To overcome this problem, the 0-0 band can be fitted assuming a two temperature rotational distribution according to the relation^{25,26}:

$$[N_J] \propto (2J + 1) \left(\text{Exp}(-F_J / kT_r^L) + R * (T_r^L / T_r^H) * \text{Exp}(-F_J / kT_r^H) \right) \quad (1)$$

where [N_J] is the density of the J rotational level, F_J is its energy, T_r^L and T_r^H are temperatures of two Boltzmann distributions, and R is the ratio of the total populations of these two distributions. T_r^L and T_r^H would correspond to distributions originating from electron impact excitation out of the ground state and to the energy transfer reaction from Ar* metastables, respectively.

To measure the gas temperature, 10% nitrogen is added to the argon feed gas and the N₂(C³Π_u- B³Π_g) 0-0 band at 337 nm is recorded with the optical detection system described in section 2, by scanning the wavelength of the monochromator. The emission intensity of several argon and copper lines is monitored to ascertain that the introduction of 10% N₂ into argon do not introduce significant perturbation on magnetron discharge. The density of ground state Cu atoms also remains unchanged. Figure 5 shows the spectra recorded at 0.6 μbar total pressure and 200 W discharge power, together with the simulated spectra according to Eq. (1). Spectra recorded with different % of N₂ have shown that within the 10 K uncertainty of the fitting procedure, the T_r^L remains unchanged when the amount of N₂ in argon is less than 20%. For the experimental conditions of Fig. 5, the neutral atoms temperature of the magnetron plasma T_a, which corresponds to the T_r^L value deduced from the two temperature fitting^{25,26}, is 320 K; the

rotational distribution in the high J levels being represented by $T_r^H = 1500$ K. For gas pressures of 0.6, 4.5 and 14 μbar , the T_a deduced from the recorded nitrogen spectra at different discharge powers are plotted in figure 6 and range between 300 and 380 K. Values at intermediate pressures can be deduced by the interpolation of these data. As expected, at fixed pressure, T_a increases with the dissipated power, but also slightly with the gas pressure²¹.

From the measurement of the Cu emission linewidth with a Fabry-Perot interferometer, Ball *et al* have reported a comparable gas temperature of 350 K in a dc copper magnetron discharge running with argon gas²⁷. Also, Kang *et al*, have reported a mean gas temperature of 300 K in pulse copper magnetron plasma²⁸. However, gas temperatures reported by Leroy *et al* in Ti magnetron plasma with argon are much higher and range between 350 and 2000 K²⁹. The first explanation for these high values could be the up to 1.5 kW dc power applied in their experiments. Another reason could be the method used by these authors, which consisted of the assumption of a Boltzmann equilibrium at gas temperature within the fine structure levels of Ti ground state atoms. But previous experiments on the time variation of the density of Ti atoms in these fine-state levels in the afterglow of a hollow cathode discharge have shown that, due to the collisional transfers by electron impact between these fine-state levels, the temperature deduced from the Boltzmann equation would provide a much higher value than the gas temperature³⁰. Gas temperatures measured by Britum *et al* in Cu and Ti magnetron argon plasmas, range between 600 and 1500 K⁷. Both techniques used by these authors - Fabry-Perot for the linewidth determination of copper and argon lines and the rotational temperature of the 2^+ bands of nitrogen added as trace gas- provided comparable results. The dc power applied in that work was apparently similar to what we have used in the present work and the much higher temperatures found in Britum's measurements can be justified by the much larger volume of our plasma chamber, hence smaller power density in our experiments than in Britum's work⁷. Also, their measurement point was located at 3 cm from the target (10 in this work) and the gas pressure range was about an order of magnitude larger. So the gas heating by fast metal atoms sputtered from the target was much more efficient in Ref. 7.

4- Resonance absorption

Determination of the ground state atoms density by resonance radiation has been developed by Mitchell and Zemansky¹⁶ and since yet the technique has been widely used by several workers^{26,28,29,31}. However, in natural copper, two isotopes: ^{63}Cu (69%) and ^{65}Cu (31%), with a nuclear spin $I = 3/2$ for both isotopes, are present. Due to the isotope shift and hyperfine structure of the levels^{32,33}, each transition has several components and the spectral profiles of the lines are quite complex. Consequently, the simple formula provided in Ref. 16 for a single line can no more be applied. In this section we will develop the formalism which must be used for the resonance absorption of multicomponent lines. The total intensity, I_0 of the line in the absence of absorption is:

$$I_0 = \int_0^\infty I_0(\nu) d\nu = \int_0^\infty \sum_i I_{0,i}(\nu) d\nu \quad (2)$$

where $I_{0,i}(\nu)$ is the incident intensity of the i component at frequency ν . When the line profile is of Doppler shape, (2) becomes³⁴:

$$I_0 = \int_0^\infty \sum_i I_{0,i}(\nu_{0,i}) \frac{2}{\Delta\nu_e} \sqrt{\frac{\ln 2}{\pi}} \cdot \text{Exp} \left[-4(\ln 2) \left(\frac{\nu - \nu_{0,i}}{\Delta\nu_e} \right)^2 \right] d\nu \quad (3)$$

where $E_i(\nu_{0,i})$ is the intensity of i component at its central frequency $\nu_{0,i}$, and $\Delta\nu_e$ is the Doppler width of the emission line from the source at temperature T_e .

$$\Delta\nu_e = \frac{2}{\lambda_0} \sqrt{\frac{2(\ln 2)kT_e}{M}} \quad (4)$$

The intensity I of the outgoing light from a homogeneously absorbing medium of length l is given by the Beer-Lambert law¹⁶:

$$I = \int_0^\infty I_0(\nu) \cdot \text{Exp}(-l \cdot k(\nu)) \cdot d\nu = \int_0^\infty \sum_i I_{0,i}(\nu) \cdot \text{Exp}(-l \cdot \sum_j k_j(\nu)) \cdot d\nu \quad (5)$$

where $k_j(\nu)$ is the frequency dependent absorption coefficient of the j component of the absorption line.

For a Doppler broadened single absorption line, the absorption coefficient is³⁴:

$$k(\nu) = \frac{1}{4\pi\epsilon_0} \frac{\pi e^2}{mc} \frac{2}{\Delta\nu_a} \sqrt{\frac{\ln 2}{\pi}} \cdot f_0 \cdot N_0 \cdot \text{Exp} \left[-4(\ln 2) \left(\frac{\nu - \nu_0}{\Delta\nu_a} \right)^2 \right] \quad (6)$$

where $\Delta\nu_a$ is the Doppler width of the absorption line in the absorbing medium at temperature T_a , N_0 is the density of absorbing atoms, f_0 is the oscillator strength of the transition and the other terms have their usual meanings. In the case of copper atom, the density of atoms N_0 is distributed between hyperfine levels of the two isotopes and for each isotope the oscillator strength f_0 is also shared between different hyperfine components of the transition. The detail of these distributions is given in Appendix A. Considering the complex spectral profiles of both emission line from the light source and absorption coefficient in the plasma, the direct determination of the absorbing atoms density from the measured absorption rate is not obvious. To overcome this difficulty, the absorption rate, $A=1-(I/I_0)$ is calculated by numerical integration of Equations (3) and (5) for different values of the absorbing atoms density, N_0 and for various couples of T_e and T_a . In this procedure, equations A3 and A4 with data of Table A1 of Appendix A are used with an absorption length, $l=20$ cm. Oscillator strengths, $f_{324}=0.439$ and $f_{327}=0.220$ are from the data base of NIST³⁵. The reported value for the green line, which is also used in this work, is $f_{510}=0.0052$. As an example, the absorption rates of 324.7 and 327.4 nm lines versus ground state Cu atoms density are shown in figure 7 for different values of the

source temperature T_e . In this figure, the absorbing atoms temperature, T_a was fixed to 330 K. With these series of curve in hand, once the values of T_a and T_e have been deduced by complementary experiments, an experimentally measured absorption rate can directly be converted to the density of absorbing atoms. We would like to emphasize that neglecting the isotopic-shift and hyperfine structures of the 324.7 nm line, as was done in Ref 28, would underestimate the density of copper atoms by about a factor of two³⁶.

5- Lamp temperature

Determination of the absorbing atoms density from the resonance absorption measurements requires the knowledge of the emission line profile of the lamp source. But the determination of this profile needs the use of a very high resolution spectrometric system (Fourier transform or Fabry-Perot interferometers with $\lambda/\delta\lambda > 10^7$), which in our cases was not available. The procedure we have followed to get rid of this problem was first to ascertain that the Doppler profile of individual lines of the light source is not distorted by autoabsorption within the hollow cathode lamp. In fact, the HCL is a hollow cylindrical copper rod, about 3 mm inner diameter and 20 mm long, in which the discharge running inside the hollow part sputters copper atoms from the cathode, which thus are excited by the discharge and emit the light containing copper transitions. As the light is observed along the tube axis, resonance photons emitted from the deepest part of the cylindrical hole can be absorbed by ground state copper atoms of the outer part of the hole. The highest probability of absorption is in fact for photons in the central part of the Doppler profile of the line. So, the spectral profile of the light coming out from the HCL can no more have a Gaussian shape and can present a deficiency in its central part. This can even lead to the self-reversal with a deep in the line center. As a result, the emission profile of a single line from the HCL will become much broader than that of a Gaussian shaped profile at the HCL temperature, with much less intensity in its central part. Higher the discharge current of the HCL, larger the density of copper atoms is and consequently stronger the distortion of the resonance line profile will be. When the gas temperature of the magnetron plasma is lower or comparable to the temperature in the HCL, as is the case in our experiments, photons of the source lamp from the edges of the frequency profile are no more, or very weakly absorbed by the copper atoms of the magnetron plasma. As a result, the intensity of the transmitted light, which is not spectrally resolved, because the spectral band-pass of the monochromator is much larger than the linewidth, will become larger than if the HCL emission line was not distorted. This phenomenon is evidenced in figure 8 which shows the variation of the normalized transmitted intensity of the 327.4 nm line versus the HCL discharge current during its on-time period. The magnetron discharge conditions were kept fixed to $p = 3.0 \mu\text{bar}$ and 210 W dc power. As expected, the ratio I/I_0 decreases with the diminution of the copper atoms density in the hollow cathode lamp, this density being directly correlated to the discharge current of the HCL. Below $i = 5 \text{ mA}$, the transmitted intensity levels off, indicating that the spectral profile of the 327.4 nm line emitted by the HCL is no more dependent on the density of Cu atoms in the light emitting region of this lamp. We should point out that at $i = 12 \text{ mA}$, increasing the discharge power of the magnetron, hence of the Cu atoms density in the magnetron plasma, had very little influence on the transmitted intensity. Meaning that the

intensity of the transmitted beam was essentially due to its spectral edges, at frequencies out of the absorption line profile, and hence a further enhancement of Cu density had no effect on it. To illustrate the influence of the HCL current on the measured density of Cu ($^2S_{1/2}$) atoms in the magnetron plasma, is shown in figure 9 the power dependence of copper density measured at $i=5$ and 12 mA, with argon pressure of 14 μ bar in the magnetron chamber. The continuous increase of the difference between two series of measurements is clearly seen in this figure. At 200 W, the estimated density with 12 mA is more than a factor of 2 smaller than the density measured at 5 mA, whereas the difference is insignificant at 10 W. In the opposite, the difference in the measured densities of Cu* ($^2D_{5/2}$) metastable atoms at 5 and 12 mA (not shown) were within the measurements uncertainty for all different magnetron plasma powers. In fact, as can be seen from the comparison of figures 3 and 4, the absorption rates are much smaller for the 510 nm line used for Cu* ($^2D_{5/2}$) atoms than for the 327.4 nm line used for Cu ($^2S_{1/2}$) atoms, the oscillator strength of the former line being about 40 times smaller than that of the 327 nm line. All data presented in the following have been obtained with 5 mA discharge current in the hollow cathode lamp.

To estimate the temperature of the Doppler profiles of the emission lines from the hollow cathode lamp, we have used an original method which consists of the comparison of the absorption rates of 324.7 and 327.4 nm lines, for which the ground state Cu ($^2S_{1/2}$) is the common lower level. The oscillator strength of 324.7 nm line being about twice that of the 327.4 nm line³⁵, the former line is much more absorbed than the 2nd one. For this purpose, we first used the procedure described in section 4 and in Appendix A to calculate for different Cu ($^2S_{1/2}$) densities ranging from 1×10^9 to 1×10^{12} cm⁻³, the absorption rates of 324.7 and 327.4 nm lines for various values of the HCL temperature, T_e . In figure 10, are plotted for $T_e= 350, 400, 500$ and 600 K the curves of the difference in the so calculated absorption rates of 324.7 and 327.4 nm lines versus the absorption rate of the 327.4 nm line. The temperature of absorbing atoms in the magnetron plasma, T_a was set to 330 K, the average value of the experimentally measured gas temperature, presented in Fig. 6. It was checked that a 10% change in T_a value will not introduce a significant modification of these theoretical plots. All of these bell-shaped curves coincide at the origin and when both absorption rates reach the unity. But they show large differences for absorption rates of the 327.4 nm line ranging between 0.3 and 0.9. In Fig. 10, are also inserted experimentally measured data points for argon pressures in the magnetron chamber of 0.6, 3 and 14 μ bar and at different applied discharge powers. They correspond to Cu ($^2S_{1/2}$) atoms densities ranging between 1 and 20×10^{10} cm⁻³, where the sensitivity of the employed procedure is high. These experimental points are all set within theoretical curves calculated for T_e values of 400 and 500 K. Consequently, all reported copper densities in the following are calculated considering a Doppler temperature of 450 K for the emission from the hollow cathode lamp. This T_e is slightly lower than what was considered in our previous works in nickel²⁶ and in titanium³⁰. But in those works, the discharge current in the HCL was also higher and probably the Doppler profiles of the emission lines slightly distorted. Konstantinidis *et al* have reported a hollow cathode lamp temperature of about 2400 K in pulsed titanium lamp³¹ above. But with 600 mA peak discharge current used in that work, the self-absorption in the HCL was certainly quite important and the emission lines from the lamp were probably not Gaussian shaped. The

same remark also applies to the lamp temperature of 800 K reported in reference 28 with 35 mA discharge current in the hollow cathode lamp.

6- Deposition rate

The deposition rate of copper (dr), measured with the quartz microbalance, is reported in figure 11 for different argon pressure and magnetron discharge power. The uncertainty on reported values is about 0.6 nm by minute. At constant pressure, the dr increases almost linearly with the dissipated discharge power. This behavior can be explained by the smallness of the change in the gas temperature with the power, which results in an almost power independent argon density in the magnetron chamber. As the neutral density controls both the energy of argon ions impinging on the target and the transport properties of the sputtered copper atoms to the substrate, the linear dependence of the deposition rate on the discharge power would indicate that in our apparatus the sputtering rate of the copper from the cathode is proportional to the discharge power. At fixed applied power, the deposition rate increases with decreasing argon pressure down to 1.5 μbar and hence remains almost unchanged between 1.5 and 0.3 μbar . It is obvious that increasing the pressure results in the diminution of the mean free path of Cu atoms in argon, thus favoring their diffusion to the chamber sidewalls and reducing the flux of Cu atoms to the substrate. But an enhancement of the plasma density with increasing pressure has been observed experimentally^{12,13}, or predicted theoretically³⁷, which consequently should increase the ion flux to the target and thus the sputtering rate of the copper. Unfortunately, using a Langmuir probe, we have not been able to carry out reliable electron density measurements in this magnetized plasma to ascertain this fact but we believe that this hypothesis should be correct. In conclusion, these two phenomena (increase of sputtering rate and simultaneous enhancement of the loss to the sidewalls when the pressure rises), which are acting in opposite directions, control the flux of Cu atoms to the substrate, thus the deposition rate. Below 1.5 μbar , they should compensate each other, leading to an almost constant deposition rate whatever the argon pressure is. Above 1.5 μbar , the plasma density should probably increase less than linearly with the gas pressure and hence the diffusion loss to the chamber walls will control the Cu flux to the substrate, resulting in the diminution of the deposition rate with increasing pressure.

7- Copper density

Figure 12 shows the magnetron discharge power dependence of copper atoms density in the ground state, Cu ($^2S_{1/2}$) (lower frame) and in the metastable state Cu* ($^2D_{5/2}$) (upper frame), measured 10 cm above the target, at different argon pressures ranging between 0.3 and 14 μbar . As a general rule, at fixed discharge power the density of Copper atoms increases with the gas pressure. This should mainly result from both enhancement with the pressure of the sputtering rate from the target and the diminution with the pressure of the volume loss of Cu atoms by diffusion to the chamber side walls, as was pointed out in previous section. But the pressure dependence trends are different for the ground state

and metastable atoms densities. At all discharge powers between 30 and 200 W, the variation of Cu density in the ground state is very close to a $p^{1/3}$ law, whereas the density in the $^2D_{5/2}$ metastable state remains nearly constant up to 1.5 μbar and then increases almost linearly with argon pressure. The change in the gas temperature with plasma parameters is very limited and one can expect a comparable diffusion coefficients of Cu ($^2S_{1/2}$) and Cu* ($^2D_{5/2}$) atoms in argon. Thus the difference in their transport properties cannot be invoked to justify the observed important difference in the pressure dependence of the densities. As we have pointed out in previous section, we expect an augmentation of the plasma density with the gas pressure and we believe that electron impact excitation of copper can influence the relative densities of the ground state and metastable atoms. The magnetron power dependence of Cu ($^2S_{1/2}$) and Cu* ($^2D_{5/2}$) densities reveals the influence of plasma parameters. As seen in Fig. 12, for argon pressures higher than 0.9 μbar , with increasing power the density of atoms in the metastable Cu* ($^2D_{5/2}$) state can even overpass the density of ground state atoms. Higher the pressure lower is the magnetron power at which the density of Cu* ($^2D_{5/2}$) atoms reaches that of the ground state atoms: around 200 W at 0.6 μbar , 130 W at 3 μbar , 110 W at 7 μbar and 70 W at 14 μbar . This evolution can be related to the variation of plasma density with either argon pressure and magnetron power and we finally come to the conclusion that the augmentation of the metastable to ground state densities ratio is directly connected to the enhancement of plasma density.

The expected electron density and temperature in this type of magnetron discharge are^{15, 38}: $n_e \cong$ a few times 10^{16} m^{-3} and $T_e \cong 1.5 - 4.5 \text{ eV}$. So, the ground state copper atoms can easily be excited by electron impact to the Cu* ($^2D_{5/2}$) metastable state, whose energy is 1.39 eV, either directly or after radiative cascades from the intermediate higher lying electronic states, in particular the resonance state $^2P_{3/2}$. Gao *et al* have used the LIF technique to measure the density of Cu ($^2S_{1/2}$) and Cu* ($^2D_{5/2}$) atoms in a magnetron argon plasma^{39, 40}. They also came to the conclusion that metastable atoms have been produced in the plasma volume by electron impact excitation of the ground state copper atoms^{40 above}. Cu atom has two metastable states: Cu* ($^2D_{5/2}$) and Cu* ($^2D_{3/2}$) and the total number of copper atoms in the non radiative long-lived states can be deduced by the addition of atom densities in the ground state and metastable states. Unfortunately, in this work it was not possible to measure the density of atoms in the other metastable Cu* ($^2D_{3/2}$) state. This was because the 578.2 nm copper line, which should be used for the absorption measurements from this state, was spoiled by the presence in the light emitted from the hollow cathode lamp of the strong 577.03 nm neon line. In fact, neon is the feed gas of the hollow cathode lamp and at 5 mA HCL current used during this work, copper lines are several orders of magnitude weaker than most of the neon lines. However, the energy separation between metastable states is only 0.25 eV^{35 above} and under our plasma conditions with $T_e \geq 1 \text{ eV}$ and $n_e \geq 1 \times 10^{16} \text{ m}^{-3}$, one can assume that electron impact collisions will equilibrate the populations of these two metastable states according to their respective statistical weights, $2J+1$. Measurements in a titanium hollow cathode plasma have shown that in the discharge period the population distribution in the fine-structure levels of the ground state a^3F_J of Ti, with $J=2, 3$ and 4, was proportional to their respective $2J+1$ values^{30 above}. But in the afterglow, after the electron temperature fallen down to the room temperature, the relative populations of the levels tended to the Boltzmann equilibrium: $N_J = (2J+1) \cdot \text{Exp}(-E_J/kT_g)$, where E_J is the energy of the fine-

structure levels of Ti and T_g is the gas temperature. If we assume population equilibrium between metastable states of Copper according to their degeneracy, and neglecting density of atoms in the high-laying excited states, whose radiative lifetimes are short³⁵, the total density of copper atoms in the long-lived states, [Cu] will be given by:

$$[Cu] = [Cu(^2S_{1/2})] + \frac{6+4}{6} \cdot [Cu^*(^2D_{5/2})] \quad (7)$$

In figure 13 are plotted the magnetron power dependence of atoms density in the ground state $^2S_{1/2}$, in the metastable state $^2D_{5/2}$ and in all long-lived states [Cu], deduced according to Equ. (7), at argon pressures 0.6, 4.5 and 14 μ bar. In this figure, are also shown the deposition rates measured at these pressures. It should be pointed out that plots of Fig. 13 are representative of the density and deposition rate evolutions at all argon pressures between 0.3 and 14 μ bar, under consideration in this work.

As seen in this figure, at fixed pressure no direct correlation can be found between the deposition rate and density of atoms in either Cu ($^2S_{1/2}$) or Cu* ($^2D_{5/2}$) states but the deposition rates seems to evolve proportionally to the total density of copper atoms [Cu]. Obviously, the constant of proportionality is a function of argon pressure on which depend the transport properties of copper atoms.

8- Conclusion

In this work, the resonance absorption technique has been used to measure the density of copper atoms in both ground state $^2S_{1/2}$ and metastable state $^2D_{5/2}$ in the middle of a magnetron discharge run with argon gas. The argon pressure varied from 0.3 to 14 μ bar and the applied dc discharge power ranged from 10 to 220 W. The complex spectral structure of the lines, resulting from the isotopic energy shift of the electronic states of Cu and of their hyperfine splitting, has been taken into account to relate the measured absorption rates to the atoms density. We have shown that the intensity of the current running the copper hollow cathode lamp, which is used as a source for the resonance absorption measurements, has a big influence on the emission spectral profiles of the copper resonance lines, hence on the absolute densities of ground state copper atoms deduced from the measured absorption rates. Under some experimental conditions, the Cu ($^2S_{1/2}$) density evaluated with a hollow cathode lamp current of 12 mA was the half of the exact density measured with 5 mA lamp current. To get rid of this artifact, originated from the self absorption of the resonance line inside the hollow cathode lamp, it was necessary to use a lamp current of 5 mA which keeps the density of ground state copper atoms low enough in the hollow cathode lamp. This finding of the influence of the HCL current renders questionable metal atom densities reported in some publications with HCL current of 35 or 20 mA^{28, 41}, or even several hundreds of mA^{29, 31, 42}.

At all Ar pressures considered in this work, for magnetron discharge power below 40 W, the density of copper atoms in the metastable state $^2D_{5/2}$ was at the detection limit and more than an order of magnitude smaller than the density of ground state copper atoms Cu ($^2S_{1/2}$). But above this limit, the metastable density increased much more rapidly with the magnetron discharge power than the density of Cu ($^2S_{1/2}$) atoms, over passing this

later around 200 W at 0.6 μbar and around 70 W at 14 μbar ; the power at which the population of both states became equal decreasing with increasing gas pressure. This behavior is attributed to the enhancement of the plasma density with both argon pressure and magnetron discharge power. So, the ground state Cu atoms are efficiently excited to the $^2\text{D}_{5/2}$ metastable state, the electron temperature in the range of 1.5 – 4.5 eV^{12, 13, 15, 37} being high enough for an efficient excitation of the $^2\text{D}_{5/2}$ state, whose threshold is 1.39 eV³⁵. Moreover, with the $2.2 \times 10^{11} \text{ cm}^{-3}$ density of Cu ($^2\text{S}_{1/2}$) atoms measured at the highest pressure and power used in this work (14 μbar and 200 W), the mean free path of 324.7 nm photons is about 5 cm, much smaller than the about 20 cm plasma dimensions. Consequently, due to the resonance radiation trapping of the 324.7 nm transition inside the plasma volume, the Holstein's theory⁴³ predicts a shortening by a factor about 5 of the effective transition probability of this line and hence Cu atoms excited to the upper level of this line, $\text{Cu}^*(^2\text{P}_{3/2})$ resonance state, will more favorably cascade down to the $\text{Cu}^*(^2\text{D}_{5/2})$ metastable state (see Fig. 1). In copper vapor laser, the emission of 510 and 578 nm laser transitions proceeds following the same scheme⁴⁴. As a result of these processes, higher the plasma density is larger the amount of atoms excited to the $\text{Cu}^*(^2\text{D}_{5/2})$ state will be.

The deposition rate of copper atoms in a substrate positioned 18 cm above the Cu target has also been measured with a quartz microbalance. At different gas pressures and magnetron discharge powers used in this work, no correlation has been found between the deposition rate and the density of ground state copper atoms measured in the middle of the plasma volume. But surprisingly, as shown in Fig. 13, the deposition rate almost follows the evolution of the total copper atoms in the ground state Cu ($^2\text{S}_{1/2}$) and metastable states $\text{Cu}^*(^2\text{D}_{5/2, 3/2})$. This observation put together with the above discussed evolution of $\text{Cu}^*(^2\text{D}_{5/2})$ atoms density lead to two important conclusions:

- A large majority of copper atoms sputtered from the target under ion bombardment are in their ground state $^2\text{S}_{1/2}$ and metastable copper atoms are produced in the plasma bulk by the electron impact excitation of ground state atoms. Gao *et al* came to the same conclusion in their study of space distribution of copper metastable atoms, detected by laser induced fluorescence technique, in a magnetron discharge⁴⁰. It should be emphasized that the outer shell electrons configuration of Cu ($^2\text{S}_{1/2}$) is $3d^{10} 4s$, similar to what is for the crystalline solid state copper, whereas the outer shell electrons configuration of Cu in both metastable states is $3d^9 4s^2$. One can speculate that during sputtering the electronic configuration of the metal is conserved.
- All copper atoms in the long-lived states, comprising ground and metastable states, contributes to the layer deposition on the substrate. The transport properties in argon of Cu atoms in various electronic states shouldn't be significantly different, so, whatever the sputtered metal atom has been excited to a metastable state or not, the deposition rate on the substrate will always be proportional to the number of sputtered atoms. Obviously, the constant of proportionality depends on the neutral gas density, *i.e.* the gas pressure and temperature. We should emphasize that in this reasoning we have assumed that the ionization rate of the metal was low enough to neglect both the contribution of Cu^+ ions to the deposition rate on the substrate and the loss of Cu atoms to the chamber walls by ambipolar diffusion of Cu^+ ions.

This above announced propensity rules should certainly also apply to other metal atoms. As an example, beside its ground state a^3F_J , titanium atom possesses seven metastable states (in reality 19 levels when accounting for the fine-structure levels with different J values), namely a^5F_J , a^1D_2 , a^3P_J , b^3F_J , a^1G_4 , a^5P_J , a^3G_J , located from 0.81 to 1.89 eV above the ground state³⁵. The total statistical weight of these metastable states ($\Sigma(2J+1)$) is 121, compared to 21 for the total statistical weight of the three fine-structure levels of the ground state. In a high density plasma with an electron temperature of a few eV, in order that electron impact excitations distribute the population according to the statistical weight of the long lifetime levels, the number density of Ti atoms in the ground state will correspond to only 15% of the total titanium atoms in the long-lived states. This fact must be accounted for when modeling the magnetron discharge or deducing the deposition rate of the metal from the measured density of ground state metal atoms.

Regarding the propensity for the sputtered atom to be in the ground state, we should mention that in nickel atoms sputtered under 8 keV argon ion bombardments, the population density of metastable a^3D_J states were comparable to that of the ground a^3F_4 state⁴⁵. But the bulk electronic configuration of Ni ($3d^84s^2$; a^3F_4) ground state is an open shell with mostly d -like rather than s - or p -like character. As a consequence, the overlap and the cross section for electron exchange between d states are considerably larger than for the s -like ground state of Ni⁴⁵. It is also possible that high energy Ar^+ ions impact induces much more violent collision cascades in the bulk, causing the excitation of the sputtered atom. Different possibilities for excitation of metastable states of metal under high energy ions impact have been extensively discussed by Nicolussi *et al*⁴⁶. In magnetron discharges the energy of impinging ions is only a few hundreds of eV. In the bulk copper as well as in the ground state of atom, the $3d^{10}$ is a closed shell and the wave function of the atom, mostly influenced by the $4s$ electron, has essentially an s -like character.

Acknowledgment

Authors would like to thank Ing. F. Hadian for his expert advices in the use of the magnetron sputtering equipment and N.S. acknowledges the Center for International Scientific Studies & Collaboration (CISSC), Iranian Ministry of Science, Research and Technology, Tehran (Iran), for the travel support to Tabriz.

Appendix A

In copper, due to the coupling of the nuclear spin, $I=3/2$ in both 63 and 65 isotopes, with the electronic angular momentum J of the considered electronic states³², the ground state $^2S_{1/2}$ splits in two hyperfine sublevels, identified by their total angular momentums $F=1$ and 2. The density of Cu atoms of the isotope k in the sublevel F'' of the ground state is

$$N_{k,F''} = \rho_k \frac{g_{F''}}{\sum_{F''} g_{F''}} N_0 \quad (\text{A1})$$

Where $g_F = 2F + 1$ is the statistical weight of the F sublevels and $\rho_k = 0.69$ and 0.31 account for the isotopic composition. Similarly, the upper states of the resonance lines, $^2P_{1/2}$ and $^2P_{3/2}$ for the 327.4 and 324.7 nm lines respectively, split in two and four sublevels, respectively, with $F=1$ and 2 for the former case and $F=3, 2, 1$ and 0 for the $^2P_{3/2}$ state. The other state of interest in this work, the $^2D_{5/2}$ metastable state -the lower level of the 510.6 nm line- also splits in four $F=4, 3, 2$ and 1 sublevels. In each transition, the oscillator strength f_0 of the line is shared between different components⁴⁷:

$$f_{F'F''} = f_0 \frac{S_{F'F''} \sum_{F''} g_{F''}}{g_{F''} \sum_{F'F''} S_{F'F''}} \quad (\text{A2})$$

where $S_{F'F''}$ are the relative line strengths and are related to $6j$ coefficients⁴⁸. Inserting A1 and A2 into equation (5), we deduce the general absorption coefficient for a multi-component Doppler broadened transition:

$$k(\nu) = \frac{2}{\Delta\nu_a} \sqrt{\frac{\ln 2}{\pi}} \frac{\pi e^2}{mc} f_0 N_0 \frac{1}{\sum_k (\rho_k \sum_{F'F''} S_{F'F''})} \times \sum_k \rho_k \sum_{F'F''} S_{F'F''} \text{Exp} \left[-4(\ln 2) \left(\frac{\nu - \nu_{F'F''}}{\Delta\nu_a} \right)^2 \right] \quad (\text{A3})$$

In summation over F' (of the upper level) and F'' (of the lower level), only couples with $\Delta F=0$ and ± 1 have to be considered, excluding 0-0 transition. Similarly, for the emission intensity of the light source, assuming statistical equilibrium between sublevels of the upper state, the spectral distribution of the line intensity is the sum of several Gaussian distributions, according to the relation:

$$I_0(\nu) = I_0 \frac{2}{\Delta\nu_e} \sqrt{\frac{\ln 2}{\pi}} \frac{1}{\sum_k (\rho_k \sum_{F'F''} S_{F'F''})} \times \sum_k \rho_k \sum_{F'F''} S_{F'F''} \text{Exp} \left[-4(\ln 2) \left(\frac{\nu - \nu_{F'F''}}{\Delta\nu_e} \right)^2 \right] \quad (\text{A4})$$

Table A1 summarizes the relative frequency shifts and emission (or absorption) intensities of different components of the 327.4, 324.7 and 510.6 nm lines. For each of these lines, the intensity of the strongest component is normalized to 100. Isotope shift of

^{63}Cu , relative to ^{65}Cu and the magnetic dipole (*A*) and electric quadrupole (*B*) momentums of the states, used to deduce relative shifts of the line components, are given in Table A2. Figures A1 to A3 show the spectral profiles of these lines at three temperatures. They correspond to the emission line profiles from the hollow cathode lamp, when the self-absorption effect can be neglected. In figure A4 is shown the spectral profile of the 327.4 nm line in the HCL light intensity transmitted from the magnetron plasma for the $\text{Cu}(^2\text{S}_{1/2})$ atoms density in the magnetron plasma ranging from 1×10^{10} to $2 \times 10^{11} \text{ cm}^{-3}$. As evidenced from this figure, at high Cu density, photons at the center of all line components are almost fully absorbed and the transmitted intensity solely comes from the edge of the absorption line profiles.

F''	F'	^{63}Cu		^{65}Cu		
		$\Delta\nu$ (MHz)	I	$\Delta\nu$ (MHz)	I	
1	0	3034	16.7	5529	7.5	510.6 nm
1	1	3258	15	5765	6.7	
1	2	3677	1.7	6210	0.8	
2	1	1909	35	4297	15.7	
2	2	2328	19.4	4742	8.7	
2	3	2885	1.1	5343	0.5	
3	2	164	62.2	2409	28	
3	3	721	15.6	3011	7	
4	3	-2423	100	-343	45	
1	1	6700	20	6636	9	327.4 nm
1	2	7713	100	7723	45	
2	1	-5033	100	-5932	45	
2	2	-4020	100	-4845	45	
1	0	6565	14.3	6468	6.4	324.7 nm
1	1	6789	35.7	6703	16	
1	2	7208	35.7	7148	16	
2	1	-4945	7.1	-5865	3.1	
2	2	-4525	35.7	-5421	16	
2	3	-3969	100	-4820	44.9	

Table A1- Frequency shift and relative intensity of different components of 510.6, 327.4 and 324.7 nm lines in both emission and absorption. For each line, the intensity of the strongest component is normalized to 100. See text for detail.

Isotope	Level	A (MHz)	B (MHz)	Isotope shift relative to ^{63}Cu (MHz)
^{63}Cu	$^2S_{1/2}$	5866.9 (a)	-	
	$^2P_{1/2}$	506.9 (b)	-	
	$^2P_{3/2}$	195.2 (c)	-28.8 (c)	
	$^2D_{5/2}$	749.1 (b)	186.0 (b)	
^{65}Cu	$^2S_{1/2}$	6284.4 (a)	-	<u>540</u> (d)
	$^2P_{1/2}$	543.3 (b)	-	0 (e)
	$^2P_{3/2}$	209.1 (c)	-26.6 (c)	-30 (e)
	$^2D_{5/2}$	803.6 (b)	174.3 (b)	-2280 (e)

Table A2- Spectroscopic constants A (electric dipole), B (magnetic quadrupole) and isotope shift of different states of Cu considered in this work.

- (a) Ting, ref. 49
- (b) Fischer et al., ref. 50
- (c) Ney, ref. 51
- (d) I Shift 2S
- (e) Ritschl, ref. 52, Wagner, ref. 53

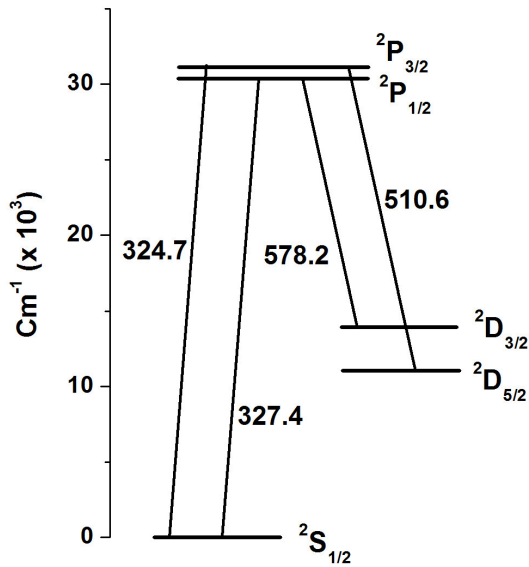


Fig.1 - Cu energy levels of interest in this work.

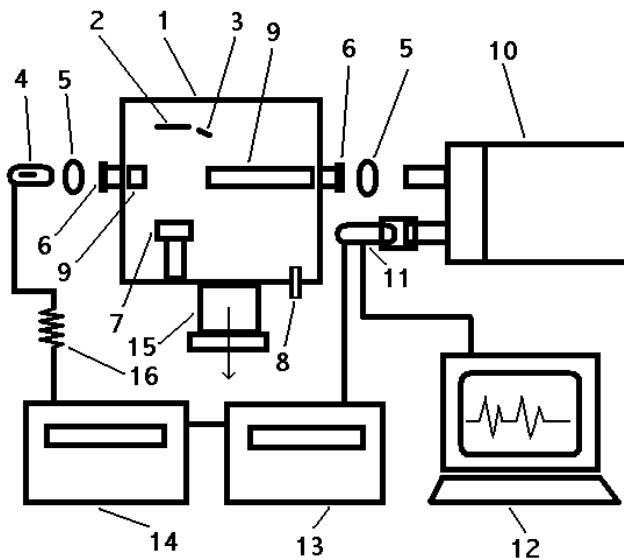


Fig.2 - Experimental Setup: 1 chamber, 2 Substrate, 3: Quartz balance, 4: HC Lamp, 5 Lens, 6: Quartz window, 7: Target, 8: Gas inlet, 9: Limiting tubes, 10: Monochromator, 11: PMT, 12: Computer, 13: Pulse generator, 14: Power supplier of the lamp, 15: Pumping orifice, 16: ballast resistor of HCL.

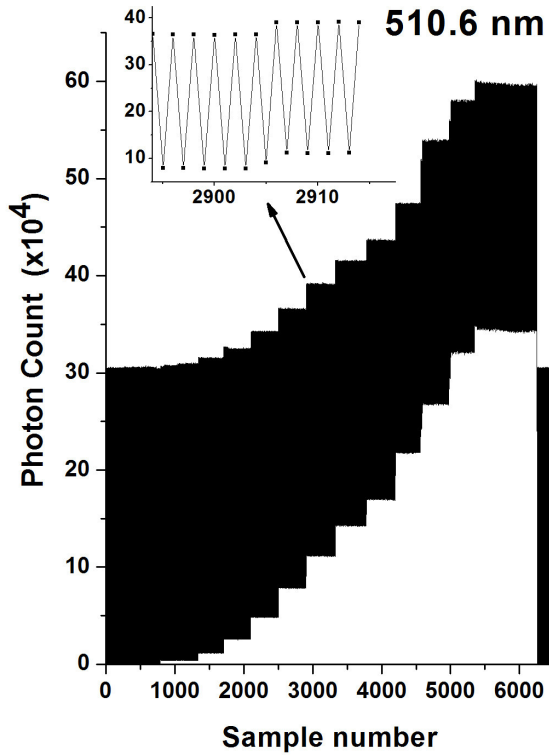


Fig.3 - Intensity of 510.6 nm line sampled every 50 ms when increasing the magnetron plasma power step by step (from left to right). The most left and the most right records are with the magnetron discharge off. One out of two samples is with the HC lamp on (upper trace) and the next is with the HC lamp off (lower trace). Data without HCL correspond to the magnetron plasma emission intensity. The inset shows an enlarged part around sample 2905, of the transition position from 70 to 80 W. Argon pressure is 14 μ bar

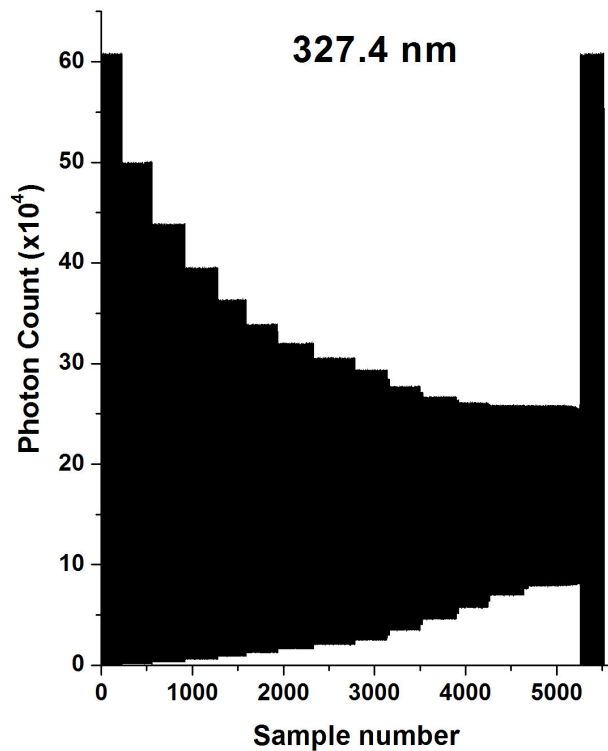


Fig.4 - Same as in Fig. 2 excepted for the 327.4 nm line. $p=0.3 \mu\text{bar}$

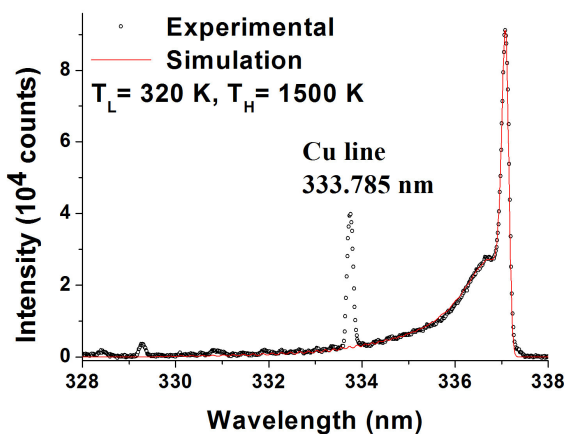


Fig.5 - (o): experimental $N_2(C^3\Pi_u - B^3\Pi_g)$ 0-0 band emission spectra with 10% N_2 added to Ar feed gas, at $p=0.6 \mu\text{bar}$ and 200 W discharge power. Two-temperature simulated spectra (red solid line), with T_L = gas temperature = 320 K (see text for detail).

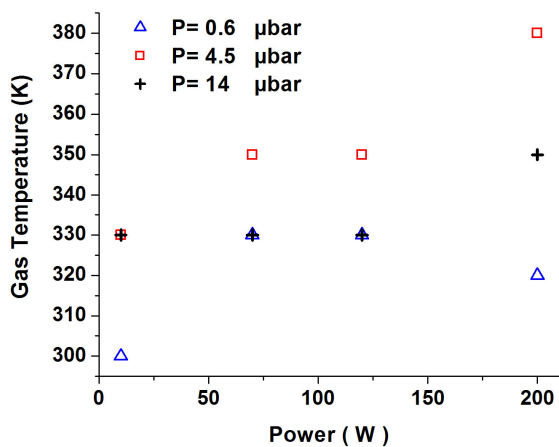


Fig.6 – Magnetron discharge power dependence of the gas temperature at 0.6, 4.5 and 14 μ bar argon pressure.

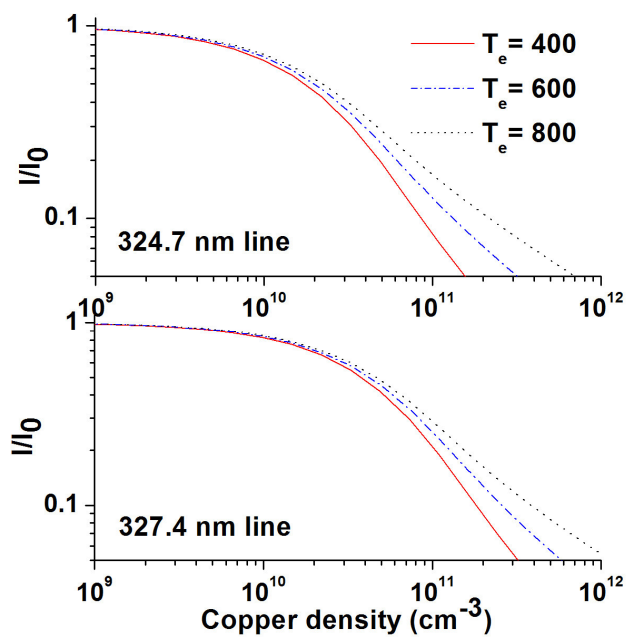


Fig.7 – The Cu density dependence of the ratio of the transmitted to the incident intensity of 324.7 and 327.4 nm lines for the HC lamp temperatures of 400, 600 and 800 K. The gas temperature in the magnetron discharge was kept at 330 K.

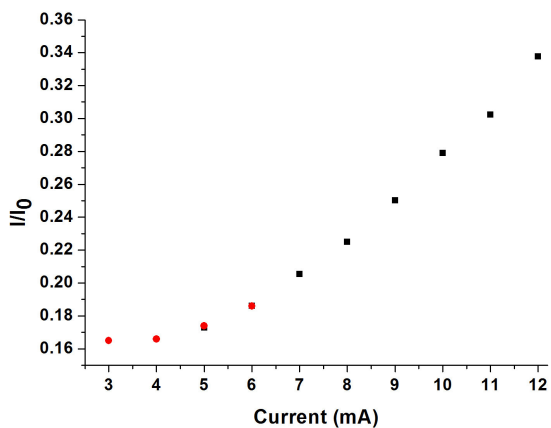


Fig.8 – Hollow cathode lamp current dependence of the ratio of the transmitted to the incident light intensities at $p= 3.0 \mu\text{bar}$ and 210 W magnetron discharge power. Red circles and black squares refer to two different data sets.

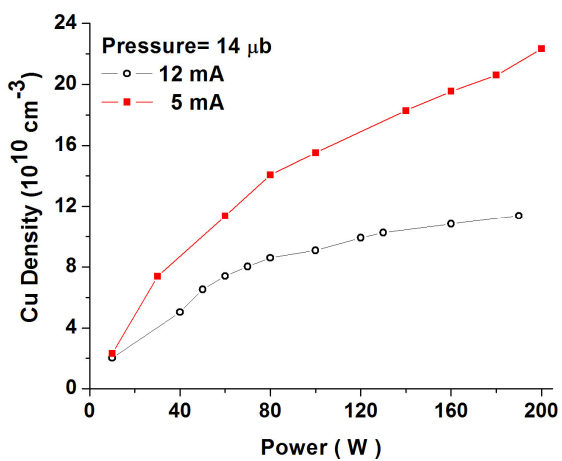


Fig.9 – Magnetron power dependence of the estimated Cu density at $14 \mu\text{bar}$ for HC lamp discharge current of 5 and 12 mA.

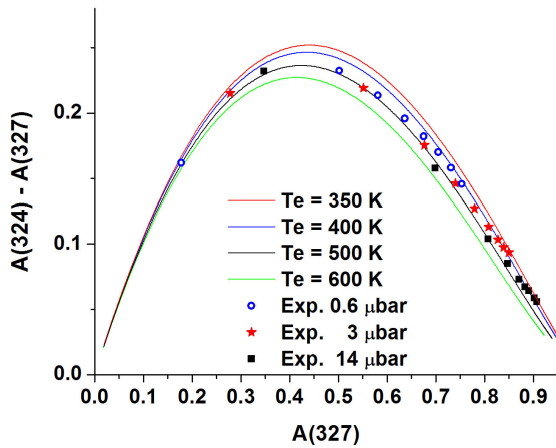


Fig.10 – Difference in absorption rates of 324.7 and 327.4 nm lines versus the absorption rate of the 327.4 nm line. Theoretical curves are for 350, 400, 500 and 600 K (down from the top, respectively). Experimental data are for different magnetron discharge powers at 0.6, 3 and 14 μbar .

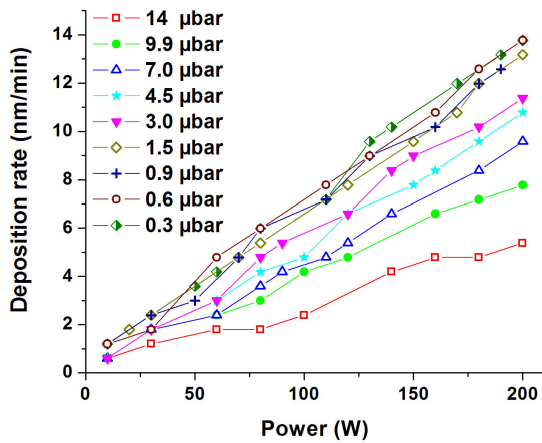


Fig.11 – Magnetron power dependence of Cu deposition rate on the substrate at argon pressures between 0.3 and 14 μbar .

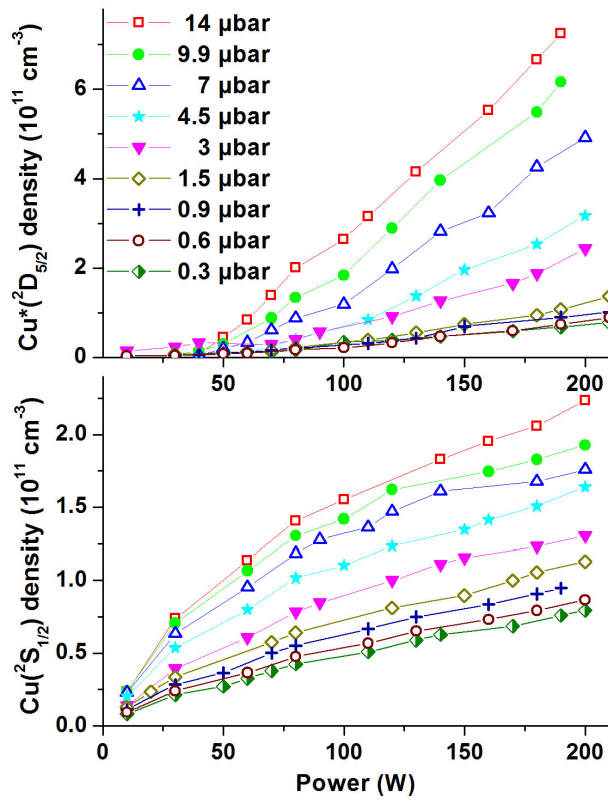


Fig.12 – Magnetron power dependence of $\text{Cu}(^2S_{1/2})$ and $\text{Cu}^*(^2D_{5/2})$ densities at argon pressures between 0.3 and 14 μbar .

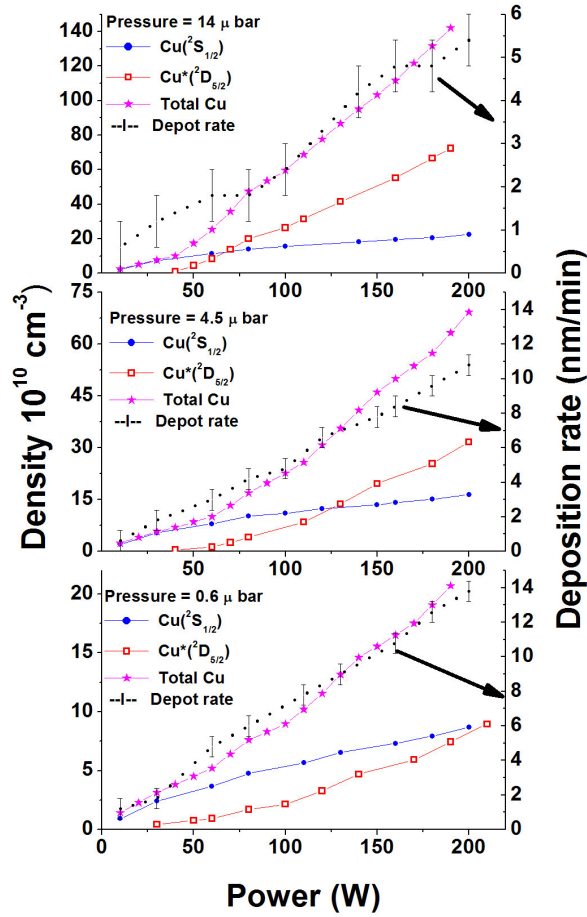


Fig.13 – Magnetron power dependence of atom density in $\text{Cu}(^2\text{S}_{1/2})$ and $\text{Cu}^*(^2\text{D}_{5/2})$ states and the total Cu atoms in the ground and metastable states (left scale) deposition rate on the substrate (right scale) at argon pressures 0.6, 4.5 and 14 μbar .

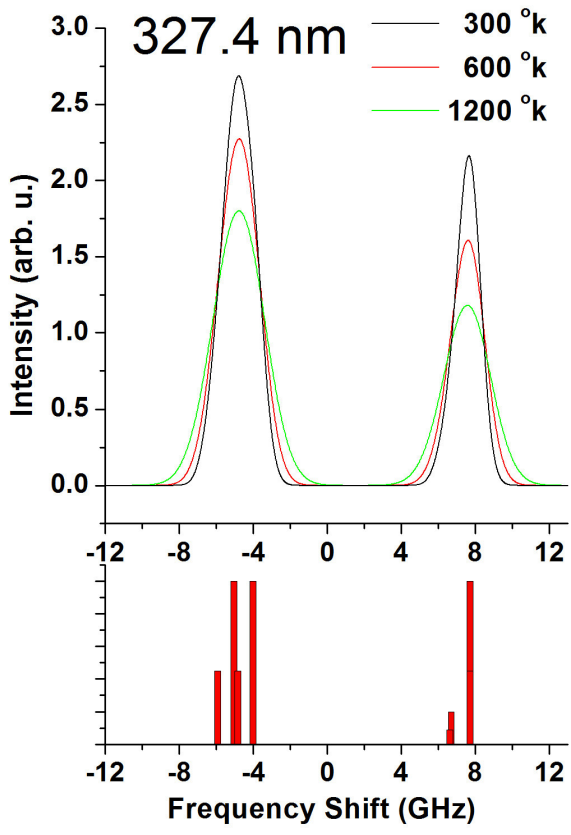


Fig.A1 – Frequency shifts and relative intensities of the 8 components of the 327.4 nm line (bottom) and the spectral profile of the line at different temperatures (top).

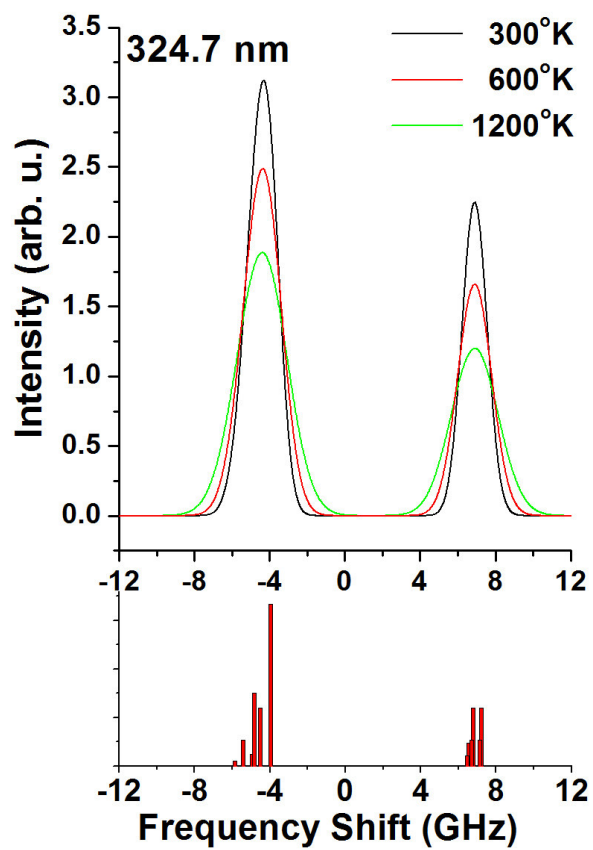


Fig.A2 – The same as Fig. A1 for 327.4 nm line, but with 12 components

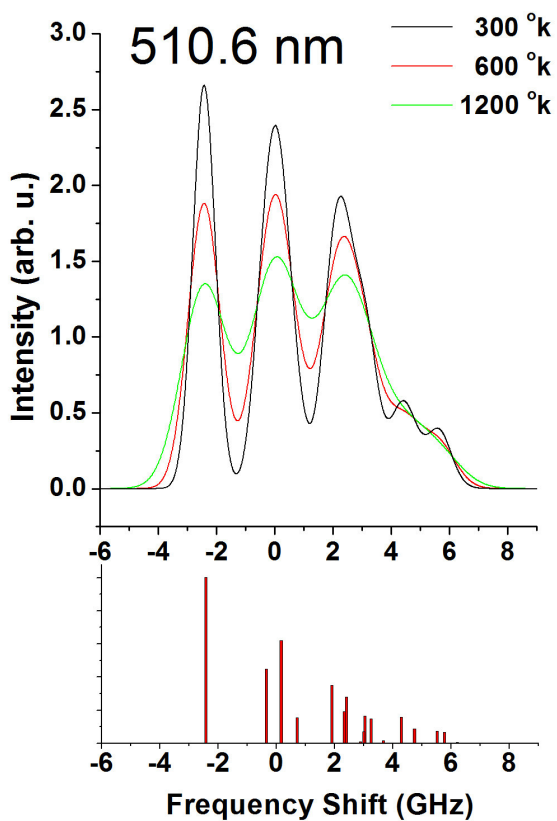


Fig.A3 – The same as Fig. A1 for 510.6 nm line, but with 18 components

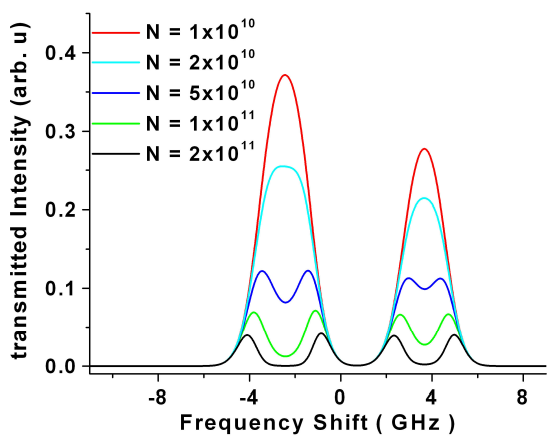


Fig.A4 – Spectral profile of the 327.4 nm line on the HCL light transmitted through the magnetron plasma at $\text{Cu}(^2\text{S}_{1/2})$ atoms density from 1 to $20 \times 10^{10} \text{ cm}^{-3}$ (from top to bottom).

References:

- ¹ Helmersson U, Lattemann M, Bohlmark J, Ehiasarian A P and Gudmundsson J T 2006 *Thin Solid Films* **513** 1
- ² Valletti K, Subrahmanyam A, Joshi S V, Phani A R, Passacantando M and Santucci S 2008 *J. Phys. D: Appl. Phys.* **41** 045409
- ³ Powell R A and Rossnagel S M 1998 *PVD for Microelectronic: Sputter Deposition Applied to Semiconductor Manufacturing* (Boston, MA: Academic)
- ⁴ Shon C H and Lee J K 2002 *Appl. Surf. Science.* **192** 258
- ⁵ Dobbertin T, Kroeger M, Heithecker D, Schneider D, Metzdorf D, Neuner H, Becker E, Johannes H H and Kowalsky W 2003 *Appl. Phys. Lett.* **82** 284
- ⁶ Karuppasamy A and Subrahmanyam A 2007 *J. Appl. Phys.* **101** 064318
- ⁷ N. Britun, M. Gaillard, S-G Oh and J.G. Han, 2007, *J. Phys. D: Appl. Phys.* **40**, 5098
- ⁸ N. Britum, J G Han and S-G Oh 2008, *Plasma Sources Sci. Technol.* **17** 045013
- ⁹ N. Britum, M. Gaillard, L. Schwaederle, Y M Kim and J G Han 2006 *Plasma Sources Sci. Technol.* **15** 790
- ¹⁰ N. Britum, M. Gaillard and J G Han 2008 *J. Phys. D: Appl. Phys.* **41** 185201
- ¹¹ K Sasaki, N Nafarizal, J-S Gao and K Shibagaki 2009 *Vacuum* **83** 463
- ¹² D J Field, S K Dew and R E Burrell 2002 *J. Vac. Sci. Technol. A*, **20**, 2032
- ¹³ P Sigurjonsson and J T Gudmundsson 2008 *Journal of Phys: Conf. Series* **100** 062018.
- ¹⁴ S-H Seo, J-H In and H-Y Chang 2004, *Plasma Sources Sci. Technol.* **13**, 409
- ¹⁵ S-H Seo, J-H In and H-Y Chang 2006, *Plasma Sources Sci. Technol.* **15**, 256.
- ¹⁶ A. C. G. Mitchell and M. W. Zemansky 1971, *Resonance Radiation and Excited Atoms*, Cambridge University Press, London.
- ¹⁷ I. Stefanovic, J. Winter and N. Sadeghi, 2010, *J. Phys. D: Appl. Phys.* **43** 152003
- ¹⁸ B. Clarenbach, B. Lorenz, M. Krämer, and N. Sadeghi, 2003 *Plasma Sources Sci. Technol.* **12** 345
- ¹⁹ L. Latrasse, N. Sadeghi, A. Lacoste, A. Bes and J. Pelletier, 2007, *J. Phys. D: Appl. Phys.* **40**, 5177
- ²⁰ D. O'Connell, T. Gans, D.L. Crintea, U. Czarnetzki and N. Sadeghi, 2008, *J. Phys. D: Appl. Phys.* **41**, 035208
- ²¹ G. Cunge, R. Ramos, D. Vempaire, M. Touzeau, M. Nejbauer, and N. Sadeghi, 2009, *J. Vac. Sci. Technol. A*, **27**, 471
- ²² V. M. Donnelly and M. V. Malyshev, 2000, *Appl. Phys. Lett.* **77**, 2467
- ²³ D. W. Setser, D. H. Stedman, and J. A. Coxon, 1970, *J. Chem. Phys.* **53**, 1004
- ²⁴ T. D. Nguyen and N. Sadeghi, 1983, *Chem. Phys.* **79**, 41
- ²⁵ Q. Wang, F. Doll, V.M. Donnelly, D.J. Economou, N. Sadeghi and G.F. Franz, 2007, *J. Phys. D: Appl. Phys.* **40**, 4202
- ²⁶ L. Xu, N. Sadeghi, V.M. Donnelly and D.J. Economou, 2007, *J. Appl. Phys.* **101**, 013304
- ²⁷ L.T. Ball, I.S. Falconer, D.R. McKenzie and J.M. Smelt, 1986, *J. Appl. Phys.* **59**, 720
- ²⁸ N. Kang, S. Oh, F. Gaboriau and A. Ricard, 2010, *Rev. Sci. Instrum.* **81**, 013102
- ²⁹ O. Leroy, L. de Poucques, C. Boisse-Laporte, M. Ganciu, L. Teule-Gay and M. Touzeau, 2004, *J. Vac. Sci. Technol. A*, **22**, 192
- ³⁰ D. Ohebsian, N. Sadeghi, C. Trassy and J.M. Mermet, 1980, *Optics Comm.* **32**, 81
- ³¹ S. Konstantinidis, A. Ricard, M. Ganciu, J.P. Dauchot, C. Ranea and M. Hecq, 2004, *J. Appl. Phys.* **95** 2900
- ³² H. Kopfermann, 1958 *Nuclear Moments* (Academic, New York).
- ³³ N. Singh and H.S. Vora, 2009, *Optics Comm.* **32**, 81
- ³⁴ N. Sadeghi, 2004, *J Plasma Fusion Res.* **80** 767
- ³⁵ <http://www.nist.gov/physlab/data/asd.cfm>
- ³⁶ P. Baltayan, F. Hartmann, I. Hikmet, and N. Sadeghi, 1992, *J. Chem. Phys.* **97**, 5417
- ³⁷ S.D. Ekpe and S.K. Dew, 2006, *J. Phys. D: Appl. Phys.* **39**, 1413
- ³⁸ N. Nafarizal, N. Takada, K. Shibagaki, K. Nakamura, Y. Sago and K. Sasaki, 2005, *Jap. J. Appl. Phys.*, **44**, L737
- ³⁹ J. Gao, N. Nafarizal and K. Sasaki, 2006, *J. Vac. Sci. Technol. A*, **24**, 2100
- ⁴⁰ J. Gao, K. Sasaki, H. Toyoda, S. Iwata and H. Sugai, 2006, *Proceedings of the 18th ESCAMPIG*, page 307.

-
- ⁴¹ A. Bogaerts, E. Wagner, B.W. Smith, J.D. Winefordner, D. Pollmann, W.W. Harrison, and R. Gijbels, 1997, *Spectrochem. Acta B* **52**, 205
- ⁴² J. Bretagne, C. Boisse Laporte, G. Gousset, O. Leroy, T.M. Minea, D. Pagnon, L. de Poucques, and M. Touzeau, 2003, *Plasma Sources Sci. Technol.* **12**, S33
- ⁴³ T. Holstein, 1947, *Phys. Rev.* **72**, 1212
- ⁴⁴ C.S. Liu, E.W. Sufov and L.A. Weaver, 1973, *Appl. Phys. Lett.* **23**, 92
- ⁴⁵ A. Cortona, W. Husinsky and G. Betz, 1999, *Phys. Rev. B* **59**, 15495
- ⁴⁶ G. Nicolussi, W. Husinsky, D. Gruber and G. Betz, *Phys. Rev. B* **51**, 8779
- ⁴⁷ W. L. Wiese, M. W. Smith, and B. M. Glennon, 1966, *Atomic Transition Probabilities* (NSRDSNBS4), Vol. 1.
- ⁴⁸ E.U. Condon and G.H. Shortley, 1935, *The Theory of Atomic Spectra*, Cambridge University Press
- ⁴⁹ Y. Ting and H. Lew, *Phys. Rev.* 1957, **105**, 581
- ⁵⁰ W. Fischer, M. Huhnermann and J.J. Kollath, 1966, *Z.f. Physik*, **194**, 417 and 1967, **200**, 159.
- ⁵¹ J. Ney, 1966, *Z.f. Physik* **196**, 53.
- ⁵² R. Ritschl, 1932, *Z.f. Physik*, **79**, 1.
- ⁵³ S. Wagner, 1955, *Z.f. Physik*, **141**, 122.